The application of the smoothed particle hydrodynamics (SPH) method to the simulation and analysis of blanking process

L. Bohdal

Koszalin University of Technology, Racławicka str. 15-17, 75-638, Koszalin, Poland, E-mail: Bohdall@interia.pl

1. Introduction

The blanking process of sheet metals has been used often to prepare workpieces for sequential forming operations. This process involves separation of the material by means of a high shear deformation due to the action of a punch. Increasing requirements concerning the cycle time, tool service life and part quality demand a better understanding of the blanking process [1-3]. Blanking is a process with geometrical and physical nonlinearities, complex thermo-mechanical and highly dynamic features. At the moment experimental studies alone have some difficulties in exploratory the deformation mechanisms during the process. Blanking modelling is becoming an very important tool in understanding and improving the methods of analysis of this processes.

In current literature the blanking numerical models are based on Lagrangian, Arbitrary Lagrangian Eulerian (ALE) or Finite Element Method (FEM) [4-9]. These approaches imply difficulties. The major difficulties are resulted from the use of grid/mesh, which can lead to various problems in dealing with free surface, moving interface, deformable boundary and crack propagation [10]. There are significant difficulties in modeling process of material failure using the element deletion method, often called element erosion. This approach leads to material mass loss, and also results in significant decrease in predicted blanking force, differences in residual stresses and strains measurement, analysis of strain state. In many cases, the generation of a quality mesh has become a difficult and time-consuming process [11]. For that reason remeshing after critical FE elements distortion is used. However, this option results in change of the crack paths and it is possible only using shell or tetrahedron elements.

Mentioned disadvantages of the finite element models can be reduced using mesh-free methods for example smoothed particle hydrodynamics (SPH). Nowadays SPH method is used not only to describe the behavior of fluids and granular materials, but also for the modeling of large plastic deformation of solids, such as simulation of the orthogonal cutting processes [12-14], shoot peening [15], guillotining [16], plastic deformation during welding [17].

In this paper, the application of mesh-free SPH methodology to the simulation and analysis of 3-D blanking process is presented. This new approach involves several advantages compared to the traditional finite element method for example: neglect mesh tangling and distortion problems, does not need to use material separation criterion. The procedure is implemented in an application created by the author using ANSYS/LS-DYNA 12.1 and LS-PrePost 2.4 programs. The main aim of the present paper is to compose the numerical model, using SPH. The model is validated with experimental research by using vision-based solutions. The proposed advanced vision-based technology is a modern tool which provide accurate measurement of sheet surface shape or deformation (displacement).

2. Basis of the SPH methhod

The idea of SPH method developed by Gingold and Monaghan [18] is to divide a continuum into discrete elements, called particles which are placed at some distance d from each other. This distance is called particle density d (Fig. 1).
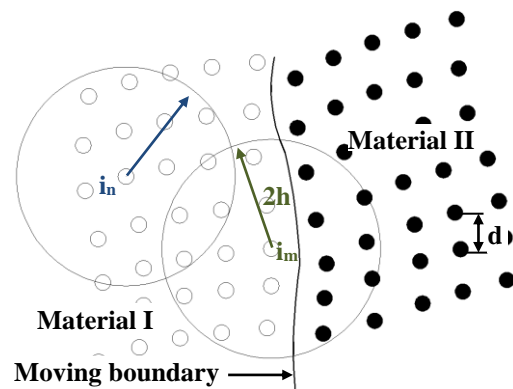

Fig. 1 Smoothing kernel in material volume and at the boundary

The field variables are smoothed by a kernel function in the area with radius h, called the smoothing length (Fig. 1). The value of a variable in any spatial point can be obtained by adding the relevant values of the variables within two smoothed lengths. The SPH approximation of the equation for continuum mechanics uses the following approaches. A body condition can be characterizing by function $f(x)$, which is substituted by its approximation $A_f(x, h)$. The velocities of a body's points in a particular area are approximated with the following expression:

$$A_f(x,h) = \int f(y)W(x,h)\,dy, \tag{1}$$

where $W(x, h)$ is a smoothed kernel function [12, 13].

The size of the smoothing kernel is defined by the function of Θ:

$$W(x,h) = \left(\frac{1}{h(x)^p}\right)\Theta(x), \tag{2}$$

where p is the dimension of space. The most common

function used by the SPH community is the cubic B-spline, determining the selection of the function Θ as follows:

$$\Theta(x) = C \begin{cases} 1 - \dfrac{3}{2}x^2 + \dfrac{3}{4}x^3, & \text{if } |x| \le 1; \\ \dfrac{1}{4}(2-x)^3, & \text{if } 1 \le |x| \le 2; \\ 0, & \text{if } 2 \le |x|, \end{cases} \qquad (3)$$

where C is the normalisation constant that depends on the number of space dimensions.

A quadratic approximation of the particle motion is mainly used for the SPH method. A motion of the particles can be described here with the following equation [12]:

$$\frac{\partial v_i^\alpha}{\partial t} = \sum_{j=1}^{N} m_j \left(\frac{\sigma_i^{\alpha\beta}}{d_i^2} + \frac{\sigma_j^{\alpha\beta}}{d_j^2} + A_{ij} \right) \frac{\partial W_{ij}}{\partial x_i^\beta}, \qquad (4)$$

where j is particle number; N is the number of neighbouring particles; $\sigma_i^{\alpha\beta}$, $\sigma_j^{\alpha\beta}$ are the stress tensors of i and j particles respectively; d_i and d_j are the densities of i and j particles respectively; $v_i^\alpha = dx_i^\alpha / dt$ is the velocity of particle i; m_j is the mass of particle j; A_{ij} are the specific external forces; $W_{ij} = W(x_i - x_j, h)$ is the smoothing kernel.

3. Coupled SPH-FEM blanking model

In the current literature the blanking simulations are mainly based on 2D FE codes. A typical blanked product has dimensions including blanking depth. Thus a full-scale 3D simulation needs to be carried out which takes into account geometrical dimension of blanked parts and length of the shearing line. The one big disadvantage of meshless methods over the Lagrangian models is their computational demand. For that reason in the suggested approach to the modeling of the blanking process, a coupling of the FEM model and the model based on hydrodynamic particles has been proposed (Fig. 2). In the case of the SPH approach, the particles are tied to the Lagrangian portion of domain using tied types of the contact. For a model with densely packed SPH nodes, it is recommended that the initial distance between the particles in each direction is approximately constant.

A velocity of $v_p = 50$ mm/s is applied to the punch in the y direction. Punch diameter is set about $d_p = 22$ mm and sheet thickness carry out $t = 4$ mm. The contact between tools and the deformable sheet metal is described using Coulomb's friction model, and constant coefficients of static friction $\mu_s = 0.08$ and kinetic friction $\mu_d = 0.009$ are accepted. Workpiece material in the simulations and experiments is 1018 steel, details are listed in Table 1. The Johnson and Cook [19, 20] material model is used to represent the constitutive behavior of the sheet. The model is often used for analysis of ductile materials in cases where strain rate vary over a large range and adiabatic temperature increase due to plastic heating cause material softening.

The model can be represented by Eq. (5):

$$\sigma_Y = \left(A + B\varepsilon^n\right)\left(1 + C \ln \dot{\varepsilon}^*\right)\left[1 - \left(\frac{T - T_r}{T_m - T_r}\right)^m\right], \qquad (5)$$

where A, B, C, n, and m are the Johnson-Cook constitutive model constants, σ is the equivalent flow stress, ε is the equivalent plastic strain, $\dot{\varepsilon}^*$ is the normalized effective plastic strain rate (typically normalized to a strain rate of 1.0 s^{-1}). T is the workpiece temperature, T_r is the room temperature, T_m is the material melting temperature.
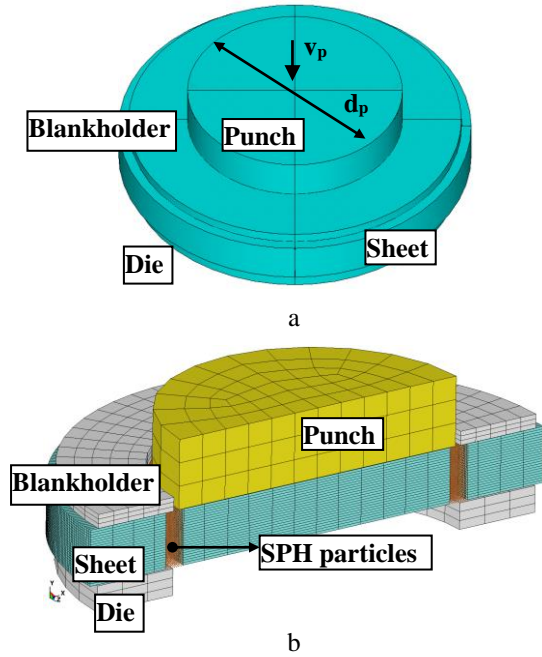

Fig. 2 FEM-SPH coupled model: a - general view; b - initial mesh of the sheet and SPH particles (cross-sectional view)

Table 1
The Johnson-Cook constitutive model constants for 1018 steel

σ_0	A	B	C	n	m
560	96	300	0.0134	0.32	1

A series of numerical simulations are carried out to determine the optimal parameters of the solver, and to obtain a minimum prediction error of blanking variables and minimal simulation cost. The computer simulations are executed for different initial particle densities: $d_1 = 0.15$ mm, $d_2 = 0.17$ mm, $d_3 = 0.19$ mm, $d_4 = 0.21$ mm, $d_5 = 0.23$ mm, $d_6 = 0.25$ mm, $d_7 = 0.27$ mm, $d_8 = 0.29$ mm, $d_9 = 0.31$ mm. A initial particle density of $d_6 = 0.25$ mm resulting in a total of 49.184 particles is selected as a optimal SPH particle density for used model dimensions. This initial particle density is selected so as to have a reasonable number of particles at the thickness of the sheet. Larger particle density not illustrate the material flow features and stress distributions appropriately, and a smaller initial particle density strongly increase the computing time. Stabilization of the stress distribution, its values and blanking force in each time step is reached when $d \le 0.25$ mm (Fig. 3). Fig. 4 shows the influence of smoothing length h on the stress distribution and its values during the plastic

flow phase. Simulations are performed for the following values of smoothing length: $h_1 = 1.05$, $h_2 = 1.1$, $h_3 = 1.2$, $h_4 = 1.3$, and $h_5 = 1.4$. It can be seen that changing the values of smoothing length between $h = 1.05 \div 1.3$ (recommended by solver options) has a small influence on stress distribution, its values and deformation state (Figs. 3 and 4). Higher values of smoothing length strongly increase the simulation time, without significant effect on maximum stress variables and deformation state during process.

Fig. 3 Stress intensity distribution in plastic flow phase of the process when $h_3 = 1.2$ for different initial particles density: a - $d_6 = 0.25$ mm (simulation time: 14 hours, 59 min); b - $d_2 = 0.17$ mm (simulation time: 73 hours, 14 min)
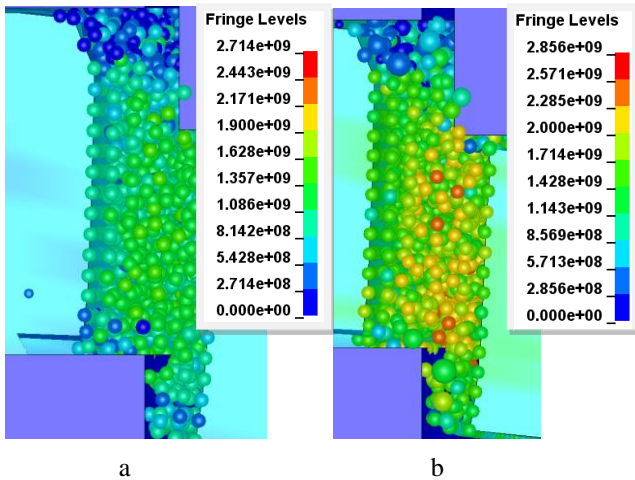

Fig. 4 Stress intensity distribution in plastic flow phase of the process for different values of smoothing length: a - $h_1 = 1.05$; b - $h_5 = 1.4$

4. Results and discussion

4.1. Blank formation

During the blanking process four main phases can be observed: elastic, elastoplastic, elastoplastic in which damage occurs, initiation and propagation of cracks leading to final rapture. During the first part of the blanking process, the punch and die indent the sheet, pulling down some surface material. The greatest deformation of material occurs near the cutting edges of the tools in this phase. In SPH-FEM model a characteristic distortion of SPH particles in this areas can be seen (Fig. 5, a). Fig. 5, b shows the image

from a high-speed camera i-SPEED TR with zoom lens used in experimental investigations in the same phase of process. During the blanking process, a camera can record a set of consecutive images of the material surface. In this work to quantify the displacements of material during and after the process, a digital image correlation technique (DIC) is used. In two-dimensional digital image correlation, displacements are directly detected from digital images of the surface of the material [21, 22]. Then, one before and another after deformation are recorded and stored in a computer disc as digital images. The images are compared by searching a salient features from one image to another for example: material texture, machining marks (image pixels), oxide deposits, finishing/polishing marks. Figs. 5, b and 5, c presents an analysis of material deformation using material texture.
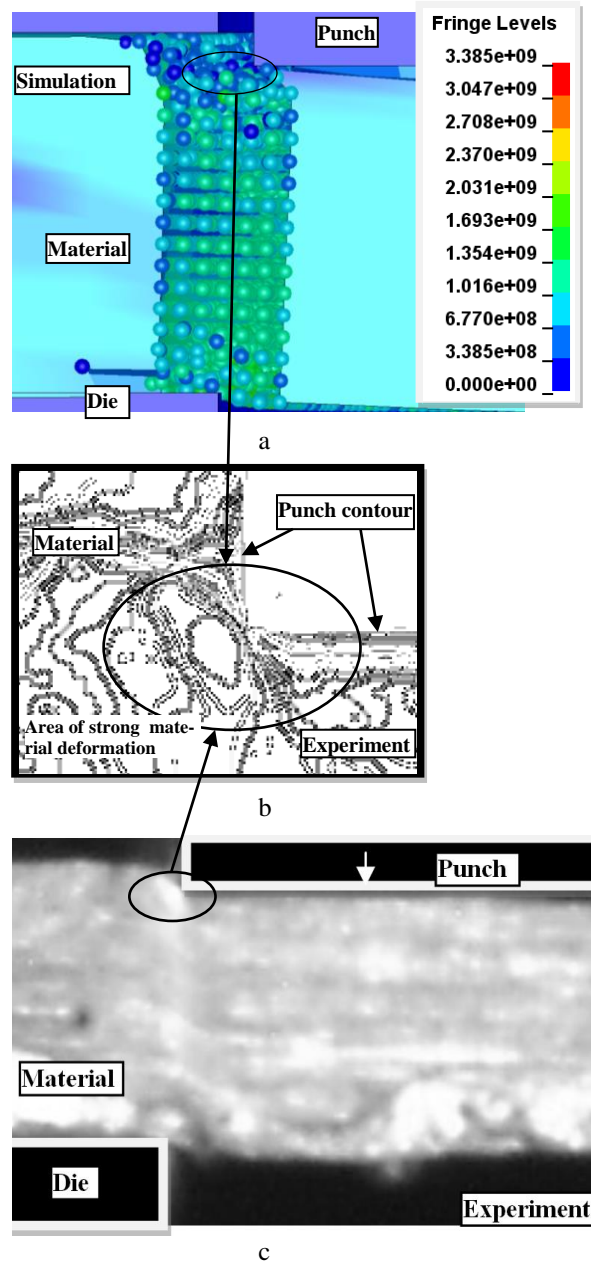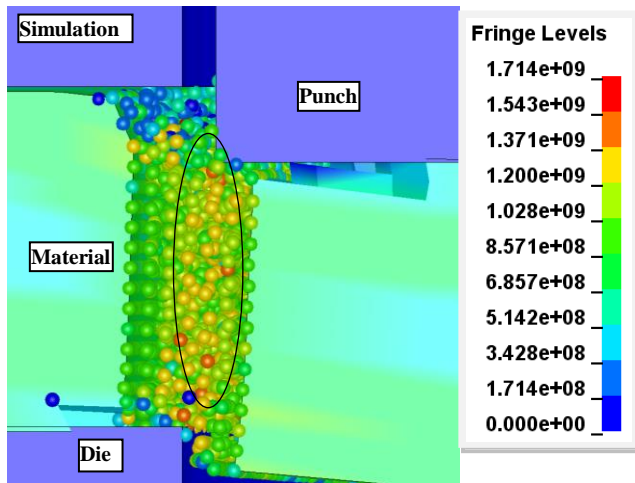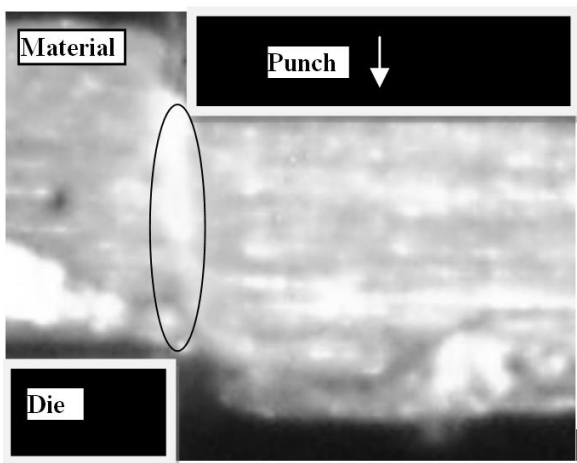

Fig. 5 Comparison of the numerical and experimental results for punch penetration $w = 0.3$ mm: a - FEM-SPH model (equivalent stress distribution); b - zoom of contact zone: image after simple feature enhancement with marked area of largest lines distortion; c - recorded image with marked contact zone (gray scale)

Fig. 5, c shows a gray scale digital image of cut material. Fig. 5, b presents punch-material contact zone after simple feature enhancement. The structure of the material can be seen as an integrated lines. Comparing the shape of lines with the lines obtained in previous image before deformation it is possible to determine the areas of strong nonlinearities and deformation of material structure.

Fig. 6 shows the next phase of blanking process which begins when the stresses within the deformation zone increases until the yield limit of the material is reached. In this phase, the extruding depth of sheet increases gradually, whilst the tensile stress and bending moment in the material continue to increase. Fig. 6, a presents the equivalent stress distribution for punch penetration $w = 0.9$ mm. It can be observed that the distortions of the SPH particles are restricted to a whole thickness of material. The highest stresses occur in the middle of the thickness of material. This tendency can be observed in experimental results. The deformation zone is extended on a whole sheet thickness which is observed on Fig. 6, b as an area with high light intensity.
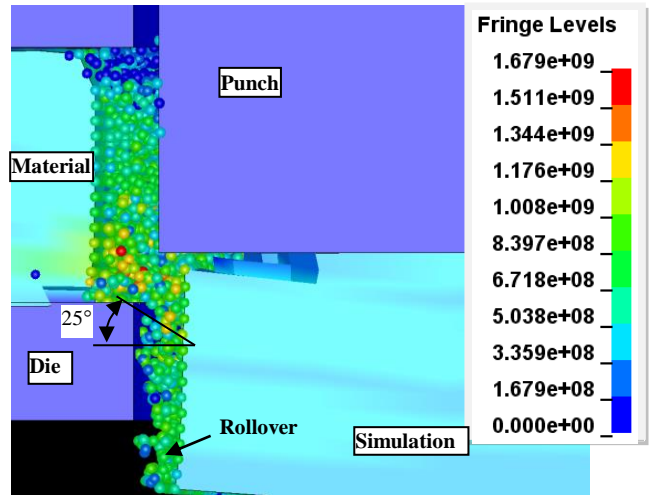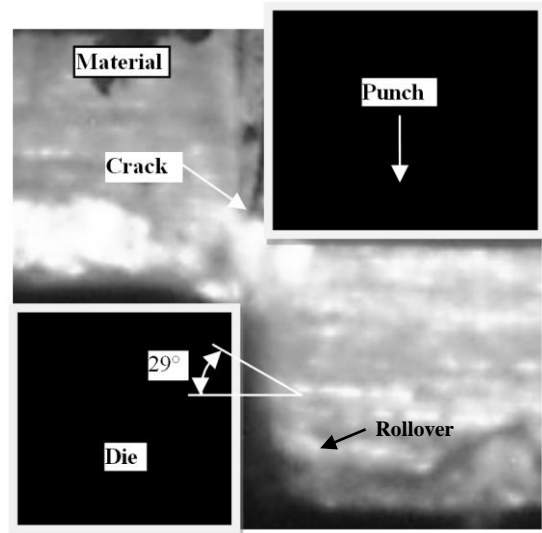

a

b

Fig. 6 Comparison of the numerical and experimental results for punch penetration $w = 0.9$ mm: a - FEM-SPH model (equivalent stress distribution); b - experiment

Fig. 7, a shows the equivalent stress distribution during the cracking phase, and measurement of flowing

angle of material with experiments (Fig. 7, b).

a

b

Fig. 7 Comparison of the numerical and experimental results for punch penetration $w = 2.9$ mm: a - FEM-SPH model (equivalent stress distribution); b - experiment

The results are in agreement with these experimental observations with approximately error margin about 4° in flowing angle of material measurement. A characteristic rollover on sheared edge can be observed. As shown on Fig. 7, b cracks of the sheet appear near to the edge of the punch. After the cracks of the top and the bottom encounter and coincide the material will separate.

4.2. Blanking force

The force-penetration curves obtained by experiment and numerical calculation are plotted in Fig. 8. The maximum value of the blanking force measured in experiment shows good agreement with the simulation results. The simulation and experimental results show that the blanking force rapidly increases at the initial stage of blanking (AB). The second stage extending from points B to C is characterized by aquasi-constant blanking force which clearly indicates the steady state of this process

stage. The last stage (*CD*) of the blanking curve corresponds to the drastic decrease of the force due to the unstable propagation of the macroscopic crack along the sheet thickness terminating the blanking operation. Some of the differences between force characteristics obtained from simulation and experiment can be seen in this phase. These differences can be explained by particle density, friction and material models, SPH velocity assumption.

4.3. Sheared edge quality

The quality of the sheared edge produced from the blanking of the sheet would depend upon the damage caused to the edge and the extent of the damage around the edge. A good shear edge quality is also correlated with a minimum burr height. In experimental investigations the optically track surface markers on the specimen during deformation is used to calculate the displacements and strains (Fig. 9).
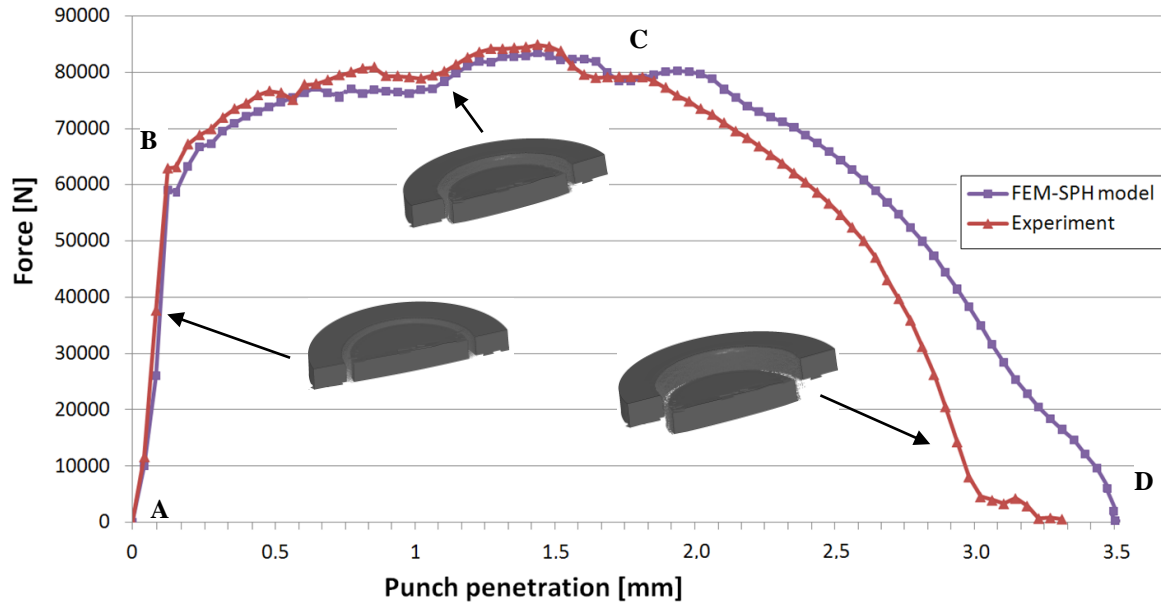

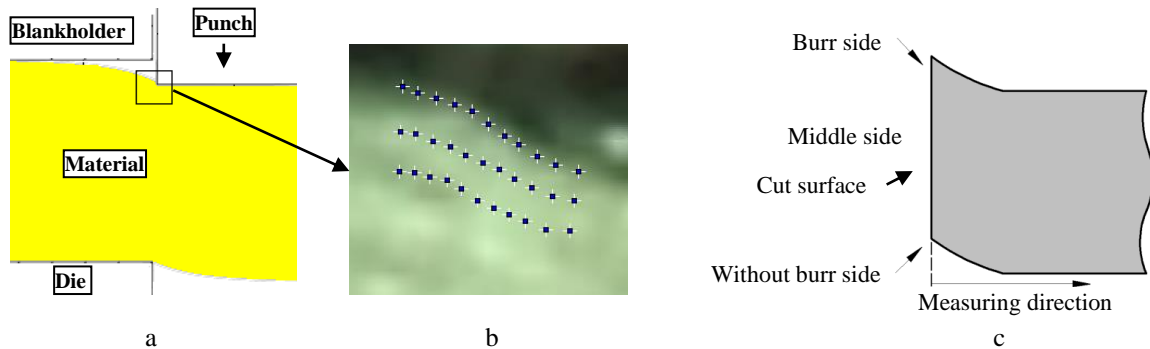Fig. 8 Comparison of the experimental and the numerical punch forces

Fig. 9 Analysis of displacements and strains distributions using DIC: a - selected area of material during process; b - example of markers pattern in damage zone; c - the three main zones of the blanked profile

All the deformed images show a different random markers pattern relative to the initial non-deformed reference image. With computer software (i-SPEED Suite) these differences between patterns are calculated by correlating all the pixels of the reference image and any deformed image, and a strain distribution is created.

It can be seen that the maximum values of plastic strain occurs at the edge and then gradually decreases with increasing distance from the cut edge until it reaches a low constant value. The measured results indicate that the maximum true strain has reached a value of 1.9 at the middle of cut surface, and it exponentially decays away from the edge. The values of strains appear to stabilize at a depth of approximately 0.75 mm (Fig. 10).

Fig. 11 shows values of normal stresses component generated on the cut surface of workpiece determined numerically, within the depth of the material in selected areas on the edge. In without burr area a high values of tension normal stress component σ_y and σ_z on sheared edge can be seen (Fig. 11, a). The stress values decrease as the distance from the edge is increasing. The stresses appear to stabilize at a depth of approximately 0.28 mm for this area. Much less normal stress component σ_y and σ_z can be observed in the middle area of sheared edge, but stresses increase with distance from the edge (Fig. 11, b). At the distance of 0.28 mm from the edge σ_y and σ_z reduce significantly and beginning to be compressive. A similar trend is observed in burr side but the normal stress component σ_y stay tensile (Fig. 11, c).
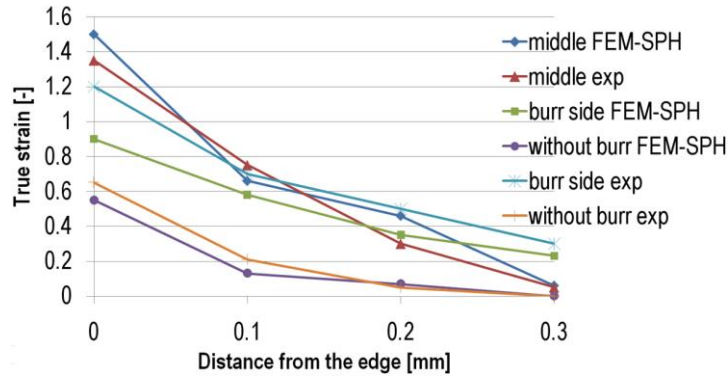
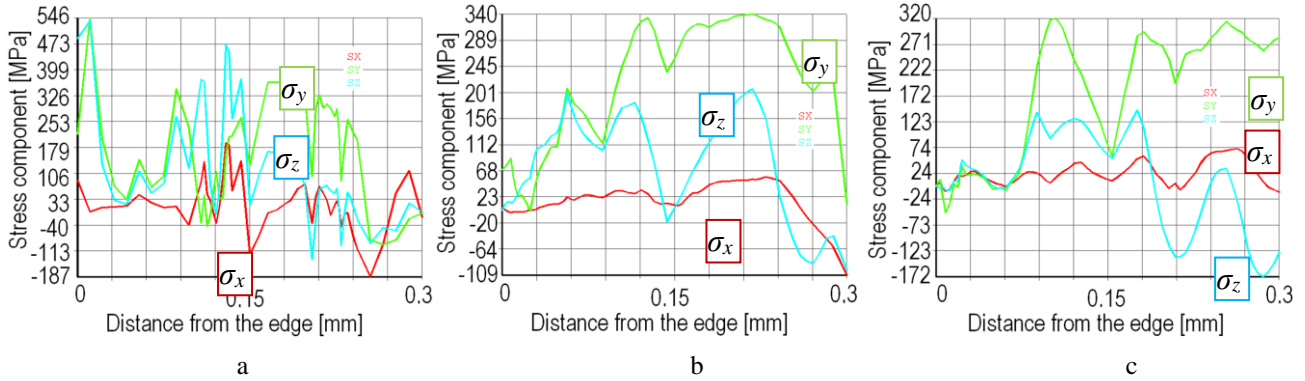Fig. 10 Results of the true strain measured in sheared edge

| a | b | c |

Fig. 11 Graphs of normal stresses component of the stress tensor depending on the distance from the sheared edge: a - without burr area; b – middle; c - burr area
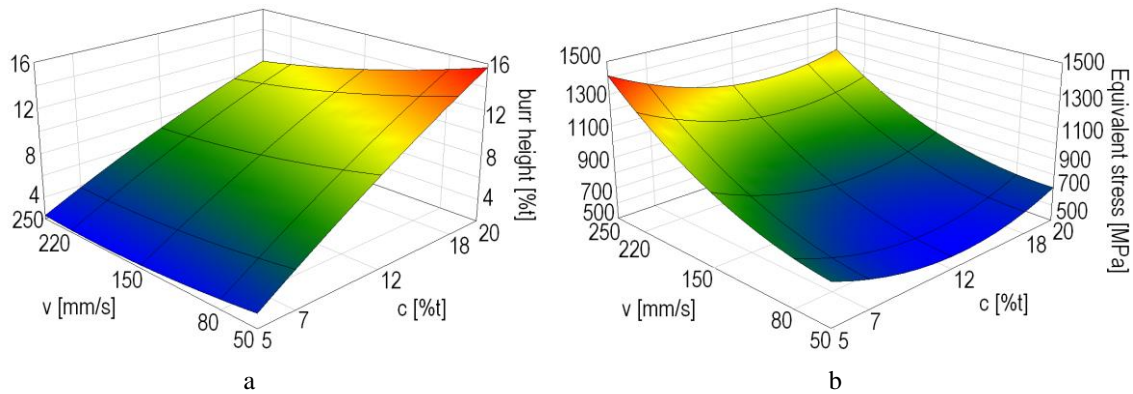

| a | b |

Fig. 12 The influence of punch velocity and clearance on: a - burr height; b - equivalent stress measured on the sheared edge

Fig. 12, a shows the effects of main process technological parameters such as the blanking velocity and clearance on the burr formation on sheared edge. The value of the burr height depends mainly on the blanking clearance value (Fig. 12, a). The maximum burr height was found using a clearance of $c = 20\%$ of sheet thickness and velocity of $v = 50$ mm/s. Reducing the clearance to $c = 5\%t$ significantly reduced the average burr height at this velocity.

It has been observed that the punch velocity has a significant influence on the equivalent stress values measured on the sheared edge (Fig. 12, b). Increasing the punch velocity increased the equivalent stress values under analysis. The maximum equivalent stress was found using a velocity of $v = 250$ mm/s and clearance of $c = 5\%t$. As the punch velocity decreases, the equivalent stress decreases (Fig. 12, b), and the small values are obtained when the clearances are set to the middle range (8-14% of the sheet thickness).

5. Conclusions

This paper presents a SPH coupled FEM method to simulate the blanking process. A hybrid approach that used the SPH formulation in the shearing zone with high material distortion and the Lagrangian formulation in the region away from the highly distorted zone is very robust and reliable. The FEM-SPH method is validated using the advanced vision based system and DIC method. Based on the experimental data, the model has been shown to be able to provide adequate estimation of the punching forces, deformation state of material and might be used for process control as well as optimizing the blanking parameters. The good agreement between simulation results and the experimental data have confirmed the correctness and credibility of the model. Actual investigations concern the simulation of blanking, in which the tools cannot be considered as rigid bodies. Further work is still required to introduce other ef-

fects concerning the behaviour of the rolled metal sheets, for example damage-induced anisotropy and spring back effects.

References

1. **Demmel, P.; Kopp, T.; Golle, R.; Volk, W.; Hoffmann, H.** 2012. Experimental investigation on the temperature distribution in the shearing zone during sheet metal blanking, Steel Research International, Special Edition on Metal Forming, 291-294. 14th International Conference on Metal Forming, Krakow, Poland.

2. **Hambli, R.** 2001. Comparison between Lemaitre and Gurson damage models in crack growth simulation during blanking process, International Journal of Mechanical Sciences 43: 2769-90.
   http://dx.doi.org/ 10.1016/S0020-7403(01)00070-4.

3. **Hambli, R.** 2001. Finite element model fracture prediction during sheet-metal blanking process, Engineering Fracture Mechanics 68: 365-378.
   http://dx.doi.org/10.1016/S0013-7944(00)00106-5.

4. **Hatanaka, N.; Yamaguchi, K.; Takakura, N.** 2003. Finite element simulation of the shearing mechanism in the blanking of sheet metal, Journal of Materials Processing Technology 139: 64-70.
   http://dx.doi.org/10.1016/S0924-0136(03)00183-3.

5. **Ko, D.C.; Kim, B.M.; Choi, J.C.** 1997. Finite-element simulation of the shear process using the element-kill method, Journal of Materials Processing Technology 72: 129-140.
   http://dx.doi.org/10.1016/S0924-0136(97)00144-1.

6. **Kwak, T.S.; Kim, Y.J.; Bae, W.B.** 2002. Finite element analysis on the effect of die clearance on shear planes in fine blanking, Journal of Materials Processing Technology 130-131: 462-468.
   http://dx.doi.org/10.1016/S0924-0136(02)00767-7.

7. **Samuel, M.** 1998. FEM simulations and experimental analysis of parameters of influence in the blanking process, Journal of Materials Processing Technology 84: 97-106.
   http://dx.doi.org/10.1016/S0924-0136(98)00083-1.

8. **Taupin, E.; Breitling, J.; Wu, WT.; Altan, T.** 1996. Material fracture and burr formation in blanking results of FEM simulations and comparison with experiments, Journal of Materials Processing Technology 59: 68-78.
   http://dx.doi.org/10.1016/0924-0136(96)02288-1.

9. **Thipprakmas, S.; Jin, M.; Kanaizuka, T.; Yamamoto, K.; Murakawa, M.** 2008. Prediction of fine blanked surface characteristics using the finite element method, Journal of Materials Processing Technology 198(1-3): 391-398.
   http://dx.doi.org/10.1016/j.jmatprotec.2007.07.027.

10. **Domski, J.; Katzer, J.** 2013. Load-deflection characteristic of fibre concrete based on waste ceramic aggregate, Annual Set The Environment Protection 15: 213-230.
    Available from Internet: http://ros.edu.pl/index.php/RO/article/view/24.

11. **Bohdal, L.; Kukielka, L.** 2014**.** Application of variational and FEM methods to the modelling and numerical analysis of guillotining process for geometrical and physical nonlinearity, Mechanika 20(2): 197-204.
    http://dx.doi.org/10.5755/j01.mech.20.2.6941.

12. **Heisel, U.; Zaloga, W.; Krivoruchko, D.; Storchak, M.; Goloborodko, L.** 2013. Modelling of orthogonal cutting processes with the method of smoothed particle hydrodynamics, Production Engineering Research and Development 7: 639-645.
    http://dx.doi.org/10.1007/s11740-013-0484-0.

13. **Bagci, E.** 2011. 3-D numerical analysis of orthogonal cutting process via mesh-free method, International Journal of Physical Sciences 6: 1267-1282.
    http://dx.doi.org/10.5897/IJPS10.600.

14. **Xi, Y.; Bermingham, M.; Wang, G.; Dargusch, M.** 2014. SPH/FE modeling of cutting force and chip formation during thermally assisted machining of Ti6Al4V alloy, Computational Materials Science 84: 188-197.
    http://dx.doi.org/10.1016/j.commatsci.2013.12.018.

15. **Jianming, W.; Feihong, L.; Feng, Y.; Gang, Z.** 2011. Shot peening simulation based on SPH method, International Journal of Advanced Manufacturing Technology 56: 571-578.
    http://dx.doi.org/10.1007/s00170-011-3193-x.

16. **Gąsiorek, D.** 2013. The application of the smoothed particle hydrodynamics (SPH) method and the experimental verification of cutting of sheet metal bundles using a guillotine, Journal of Theoretical and Applied Mechanics 51(4): 1053-1065.
    Available from Internet: http://www.ptmts.org.pl/2013-4-gasiorek.pdf.

17. **Das, R.; Cleary, P.W.** 2007. Modeling plastic deformation and thermal response in welding using smoothed particle hydrodynamics, 16th Australasian fluid mechanics conference, 2–7 December 2007.
    Available from Internet: https://espace.library.uq.edu.au/view/UQ:120786/Das_afmc_16_07.pdf.

18. **Gingold, R.A.; Monaghan, J.J.** 1977. Smooth particle hydrodynamics: theory and application to non-spherical stars, Monthly Notices of the Royal Astronomical Society 181: 375-389.
    http://dx.doi.org/10.1093/mnras/181.3.375.

19. **Johnson, G.R.; Cook, W.H.** 1985. Fracture characteristics of three metals subjected to various strains, strain rates, temperatures and pressures, Engineering Fracture Mechanics 21(1): 31-48.
    http://dx.doi.org/10.1016/0013-7944(85)90052-9.

20. **Malag, L.; Kukielka, L.; Kukielka, K.; Kulakowska, A.; Bohdal, L.; Patyk, R.** 2014. Problems determining of the mechanical properties of metallic materials from the tensile test in the aspect of numerical calculations of the technological processes, Applied Mechanics and Materials 474: 454-459.
    http://dx.doi.org/10.4028/www.scientific.net/AMM.474.454.

21. **Yoneyama, S.; Kitagawa.; Kitamura, K.; Kikuta, H.** 2006. In-plane displacement measurement system using digital image correlation with lens distortion correction, JSME International Journal, Series A, 49(3): 458-467.
    http://dx.doi.org/10.1299/jsmea.49.458.

22. **Kozicki, J.; Tejchman, J.** 2007. Experimental investigations of strain localization in concrete using digital image correlation (DIC) technique, Archives of Hydro-Engineering and Environmental Mechanics 54(1): 3-24.
    Available from Internet: http://www.ibwpan.gda.pl/docs/ahem/ahem54str003.pdf.

L. Bohdal

THE APPLICATION OF THE SMOOTHED PARTICLE HYDRODYNAMICS (SPH) METHOD TO THE SIMULATION AND ANALYSIS OF BLANKING PROCESS

S u m m a r y

In this paper, the applications of mesh-free SPH (Smoothed Particle Hydrodynamics) methodology to the simulation and analysis of 3-D blanking process is presented. This approach allows for a complex analysis of physical phenomena occurring during the process without significant deterioration in the quality of the finite element mesh during large deformation. This allows for accurate representation of the loss of cohesion of the material under the influence of punch and die. An analysis of state of stress, strain and fracture mechanisms of the material is presented. In experimental studies, an advanced vision-based technology based on digital image correlation (DIC) for monitoring the blanking process is used.